Aust. J. Phys., 1993, **46**, 37–59

Single Atom Experiments and the Test of Quantum Physics*

H. Walther

Sektion Physik der Universität München and
Max-Planck-Institut für Quantenoptik,
Postfach 1513, 8046 Garching, Germany.

Abstract

In this paper experiments performed with a one-atom maser and with a few ions stored in a Paul trap are reviewed. Special emphasis is placed on experiments for the test of quantum physics.

1. Introduction

In recent years single-atom experiments have become possible. In this paper two groups of these experiments will be reviewed with special emphasis on applications to the study of quantum phenomena. The first group deals with the one-atom maser and the second with the application of trapped ions (Wineland *et al.* 1984). In recent years there has also been considerable progress in trapping neutral atoms (Chu *et al.* 1986; Pritchard *et al.* 1988). This technique is very promising and is undergoing rapid development. So far, however, no experiments have been performed to test quantum physics with this method; therefore this technique will not be discussed in detail here.

2. Review of the One-atom Maser

The most promising avenue to study the generation process of radiation in lasers and masers is to drive a maser consisting of a single mode cavity by single atoms. This system, at first glance, seems to be another example of a Gedanken-experiment but such a one-atom maser (Meschede *et al.* 1985) really exists and can in addition be used to study the basic principles of the radiation–atom interaction. The advantages of the system are:
(1) it is the first maser which sustains oscillations with less than one atom on the average in the cavity,
(2) this setup allows one to study in detail the conditions necessary to obtain nonclassical radiation, especially radiation with sub-Poissonian photon statistics, in a maser system directly, and
(3) it is possible to study a variety of phenomena of a quantum field including the quantum measurement process.

* Paper presented at the Tenth AIP Congress, University of Melbourne, February 1992.

0004-9506/93/010037$05.00

What are the tools that make this device work? It is the enormous progress in constructing superconducting cavities together with the laser preparation of highly excited atoms—Rydberg atoms—that have made the realisation of such a one-atom maser possible. Rydberg atoms have quite remarkable properties (Haroche and Raimond 1985; Gallas *et al.* 1985) which make them ideal for such experiments: the probability of induced transitions between neighbouring states of a Rydberg atom scales as n^4, where n denotes the principal quantum number. Consequently, a few photons are enough to saturate the transition between adjacent levels. Moreover, the spontaneous lifetime of a highly excited state is very large. We obtain a maser by injecting these Rydberg atoms into a superconducting cavity with a high quality factor. The injection rate is such that on the average there is less than one atom present inside the resonator at any time. A transition between two neighbouring Rydberg levels is resonantly coupled to a single mode of the cavity field. Due to the high quality factor of the cavity, the radiation decay time is much longer than the characteristic time of the atom–field interaction, which is given by the inverse of the single-photon Rabi frequency. Therefore it is possible to observe the dynamics (Jaynes and Cummings 1963) of the energy exchange between atom and field modes leading to collapses and revivals in the Rabi oscillations (Eberly *et al.* 1980; Rempe *et al.* 1987). Moreover, a field is built up inside the cavity when the mean time between the atoms injected into the cavity is shorter than the cavity decay time.

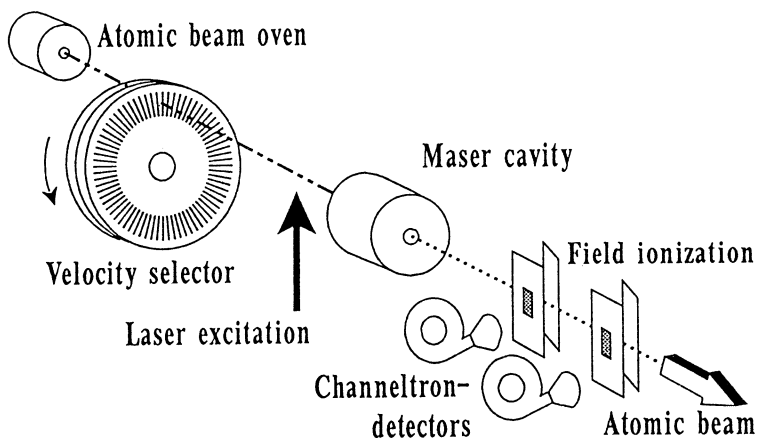

Fig. 1. Scheme of the one-atom maser. To suppress blackbody-induced transitions to neighbouring states, the Rydberg atoms are excited inside the liquid-helium-cooled environment.

The detailed experimental setup of the one-atom maser is shown in Fig. 1. A highly collimated beam of rubidium atoms passes through a Fizeau velocity selector. Before entering the superconducting cavity, the atoms are excited into the upper maser level $63p_{3/2}$ by the frequency-doubled light of a cw ring dye laser. The laser frequency is stabilised onto the atomic transition $5s_{1/2} \rightarrow 63p_{3/2}$, which has a width determined by the laser linewidth and the transit-time broadening corresponding to a total of a few MHz. In this way, it is possible to prepare a very stable beam of excited atoms. The ultraviolet light is linearly polarised

parallel to the electric field of the cavity. Therefore only $\Delta m = 0$ transitions are excited by both the laser beam and the microwave field. The superconducting niobium maser cavity is cooled down to a temperature of 0·5 K by means of a ^{3}He cryostat. At this temperature the number of thermal photons in the cavity is about 0·15 at a frequency of 21·5 GHz. The cryostat is carefully designed to prevent room temperature microwave photons from leaking into the cavity. This would considerably increase the temperature of the radiation field above the temperature of the cavity walls. The quality factor of the cavity is 3×10^{10} corresponding to a photon storage time of about 0·2 s. The cavity is carefully shielded against magnetic fields by several layers of cryoperm. In addition, three pairs of Helmholtz coils are used to compensate the earth's magnetic field to a value of several mG in a volume of $10\times4\times4$ cm^3. This is necessary in order to achieve the high quality factor and prevent the different magnetic substates of the maser levels from mixing during the atom–field interaction time. Two maser transitions, from the $63p_{3/2}$ level to the $61d_{3/2}$ and $61d_{5/2}$ levels, are studied.

The Rydberg atoms in the upper and lower maser levels are detected in two separate field ionisation detectors. The field strength is adjusted so as to ensure that in the first detector the atoms in the upper level are ionised, but not those in the lower level. The lower level atoms are then ionised in the second field.

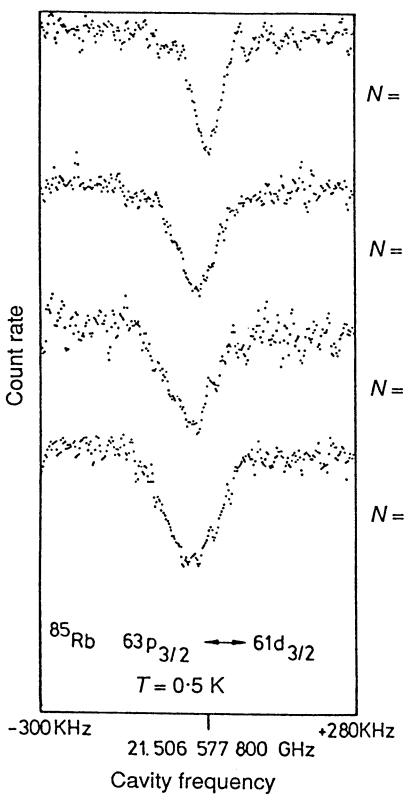

Fig. 2. A maser transition of the one-atom maser manifests itself in a decrease in the number of atoms in the excited state. The flux of excited atoms N governs the pump intensity. Power broadening of the resonance line demonstrates the multiple exchange of a photon between the cavity field and the atom passing through the resonator.

To demonstrate maser operation, the cavity is tuned over the $63p_{3/2}$–$61d_{3/2}$ transition and the flux of atoms in the excited state is recorded simultaneously. Transitions from the initially prepared $63p_{3/2}$ state to the $61d_{3/2}$ level (21·50658 GHz) are detected by a reduction of the electron count rate.

In the case of measurements at a cavity temperature of 0·5 K, shown in Fig. 2, a reduction of the $63p_{3/2}$ signal can be clearly seen for atomic fluxes as small as 1750 atoms/s. An increase in flux causes power broadening and a small shift. This shift is attributed to the ac Stark effect, caused predominantly by virtual transitions to neighbouring Rydberg levels. Over the range from 1750 to 28000 atoms/s the field ionisation signal at resonance is independent of the particle flux, which indicates that the transition is saturated. This result and the observed power broadening show that there is a multiple exchange of photons between Rydberg atoms and the cavity field.

For an average transit time of the Rydberg atoms through the cavity of 50 μs and a flux of 1750 atoms/s, we estimate that approximately 0·09 Rydberg atoms are in the cavity on the average. According to Poisson statistics this implies that more than 90% of the events are due to single atoms. This clearly demonstrates that single atoms are able to maintain a continuous oscillation of the cavity with a field corresponding to a mean number of photons between unity and several hundred.

3. A New Source of Nonclassical Light

One of the most interesting questions in connection with the one-atom maser concerns the photon statistics of the electromagnetic field generated in the superconducting cavity. This problem will be discussed in this section.

Electromagnetic radiation can show nonclassical properties (Walls 1979, 1983, 1986), that is, properties that cannot be explained by classical probability theory. Loosely speaking, we need to invoke 'negative probabilities' to get deeper insight into these features. We know of essentially three phenomena which demonstrate the nonclassical character of light: photon antibunching (Kimble *et al.* 1977; Cresser *et al.* 1982), sub-Poissonian photon statistics (Short and Mandel 1983) and squeezing (Slusher *et al.* 1985; Loudon and Knight 1987). Mostly methods of nonlinear optics are employed to generate nonclassical radiation. However, the fluorescence light from a single atom caught in a trap also exhibits nonclassical features (Carmichael and Walls 1976; Diedrich and Walther 1987).

Another nonclassical light generator is the one-atom maser. We recall that the Fizeau velocity selector preselects the velocity of the atoms: hence the interaction time is well-defined which leads to conditions usually not achievable in standard masers (Filipowicz *et al.* 1986*a–c*; Lugiato *et al.* 1987; Krause *et al.* 1987, 1989; Meystre 1987; Meystre *et al.* 1988; Slosser *et al.* 1990). This has a very important consequence when the intensity of the maser field grows as more and more atoms give their excitation energy to the field. Even in the absence of dissipation this increase in photon number is stopped when the increasing Rabi frequency leads to a situation where the atoms reabsorb the photon and leave the cavity in the upper state. For any photon number, this can be achieved by appropriately adjusting the velocity of the atoms. In this case the maser field is not changed any more and the number distribution of the photons in the cavity is sub-Poissonian (Filipowicz *et al.* 1986*a–c*; Lugiato *et al.* 1987), that is, narrower than a Poisson distribution. Even a number state that is a state of well-defined photon number can be generated (Krause *et al.* 1987, 1989; Meystre 1987) using a cavity with a high enough quality factor. If there are no thermal photons in the cavity—a condition achievable by cooling the resonator to an extremely low temperature—very interesting features such as trapping states show up (Meystre

et al. 1988). In addition, steady-state macroscopic quantum superpositions can be generated in the field of the one-atom maser pumped by two-level atoms injected in a coherent superposition of their upper and lower states (Slosser *et al.* 1990).

Unfortunately, the measurement of nonclassical photon statistics in the cavity is not that straightforward. The process of measuring the field invokes coupling to a measuring device, with losses leading inevitably to a destruction of the nonclassical properties. The ultimate technique to obtain information about the field employs the Rydberg atoms themselves: one possibility is to measure the photon statistics via the dynamic behaviour of the atoms in the radiation field, i.e., via the collapse and revival of the Rabi oscillations. However, since the photon statistics depend on the interaction time, which has to be changed when collapse and revival are measured, it is much better to probe the population of the atoms in the upper and lower maser levels when they leave the cavity. In this case the interaction time is kept constant. Moreover, this measurement is relatively easy since electric fields can be used to perform selective ionisation of the atoms. The detection sensitivity is sufficient that the atomic statistics can be investigated. This technique maps the photon statistics of the field inside the cavity via the atomic statistics.

In this way the number of maser photons can be inferred from the number of atoms detected in the lower level (Meschede *et al.* 1985). In addition, the variance of the photon number distribution can be deduced from the number fluctuations of the lower-level atoms (Rempe and Walther 1990). In the experiment, we are therefore mainly interested in the atoms in the lower maser level. Experiments carried out along these lines are described in the following section.

4. Experimental Results—A Beam of Atoms with Sub-Poissonian Statistics

Under steady state conditions, the photon statistics of the field are essentially determined by the dimensionless parameter $\Theta = (N_{ex} + 1)^{1/2}\Omega t_{int}$, which can be understood as a pump parameter for the one-atom maser (Filipowicz *et al.* 1986*a–c*). Here, N_{ex} is the average number of atoms that enter the cavity during the lifetime of the field T_c, t_{int} is the time of flight of the atoms through the cavity, and Ω is the atom–field coupling constant (one-photon Rabi frequency). The one-atom maser threshold is reached for $\Theta = 1$. At this value and also at $\Theta = 2\pi$ and integer multiples thereof, the photon statistics are super-Poissonian. At these points the maser field undergoes first-order phase transitions (Filipowicz *et al.* 1986*a–c*). In the regions between these points sub-Poissonian statistics are expected. The experimental investigation of the photon number fluctuation is the subject of the following discussion.

In the experiments (Rempe *et al.* 1990), the number N of atoms in the lower maser level is counted for a fixed time interval T roughly equal to the storage time T_c of the photons. By repeating this measurement many times the probability distribution $p(N)$ of finding N atoms in the lower level is obtained. The normalised variance (Mandel 1979) $Q_a = [\langle N^2\rangle - \langle N\rangle^2 - \langle N\rangle]/\langle N\rangle$ is evaluated and used to characterise the deviation from Poissonian statistics. A negative (positive) Q_a value indicates sub-Poissonian (super-Poissonian) statistics, while $Q_a = 0$ corresponds to a Poisson distribution with $\langle N^2\rangle - \langle N\rangle^2 = \langle N\rangle$. The atomic Q_a is related to the normalised variance Q_f of the photon number by the formula

$$Q_a = \epsilon P Q_f (2 + Q_f)\,, \tag{1}$$

which was derived by Rempe and Walther (1990), with P denoting the probability of finding an atom in the lower maser level. It follows from equation (1) that the nonclassical photon statistics can be observed via sub-Poissonian atomic statistics. The detection efficiency ϵ for the Rydberg atoms reduces the sub-Poissonian character of the experimental result. The detection efficiency was 10% in our experiment; this includes the natural decay of the Rydberg states between the cavity and field ionisation. It was determined by both monitoring the power-broadened resonance line as a function of flux (Meschede *et al.* 1985) and observing the Rabi oscillation for constant flux but different atom–field interaction times (Rempe *et al.* 1987). In addition, this result is consistent with all other measurements described in the following, especially with those on the second maser phase transition.

Experimental results for the transition $63p_{3/2} \leftrightarrow 61d_{3/2}$ are shown in Fig. 3. The measured normalised variance Q_a is plotted as a function of the flux of atoms. The atom–field interaction time is fixed at $t_{int} = 50$ μs. The atom–field coupling constant is rather small for this transition, $\Omega = 10$ kHz. A relatively high flux of atoms, $N_{ex} > 10$, is therefore needed to drive the one-atom maser

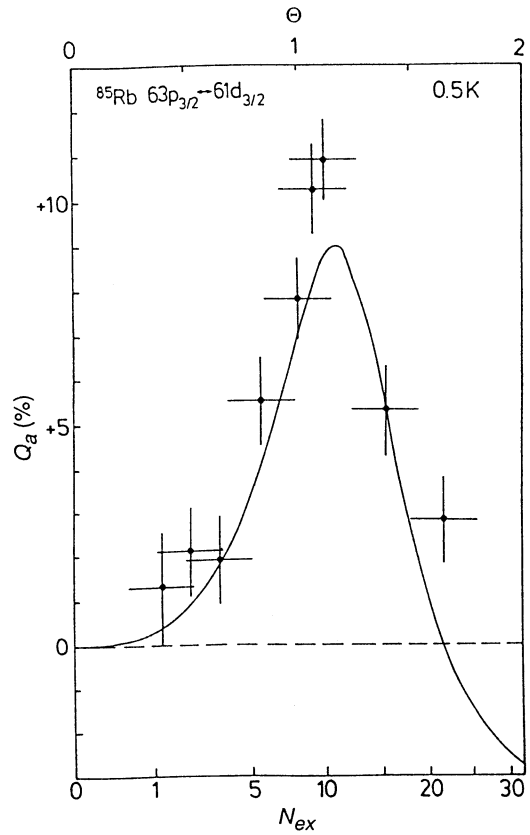

Fig. 3. Variance Q_a of the atoms in the lower maser level as a function of flux N_{ex} near the onset of maser oscillation for the $63p_{3/2} \leftrightarrow 61d_{3/2}$ transition (Rempe *et al.* 1990).

above threshold. The large positive Q_a observed in the experiment proves the large intensity fluctuations at the onset of maser oscillation at $\Theta = 1$. The solid curve is plotted according to equation (1) using the theoretical predictions for Q_f of the photon statistics (Filipowicz *et al.* 1986*a–c*; Lugiato *et al.* 1987). The error in the signal follows from the statistics of the counting distribution $p(N)$. About $2{\times}10^4$ measurement intervals are needed to keep the error of Q_a below 1%. The statistics of the atomic beam are measured with a detuned cavity. In this case the regular statistics of the atomic beam are measured which corresponds to Poissonian statistics. The error bars of the flux follow from this measurement. The agreement between theory and experiment is good.

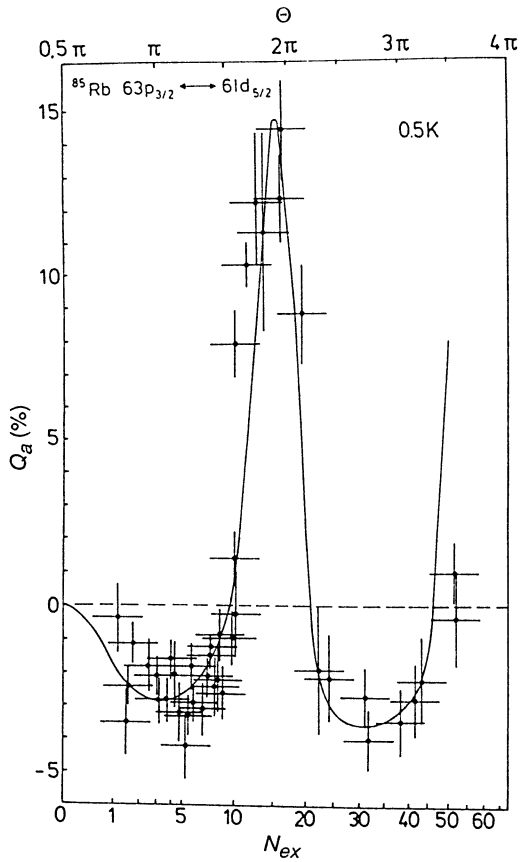

Fig. 4. Same as Fig. 3, but above threshold for the $63p_{3/2} \leftrightarrow 61d_{5/2}$ transition (Rempe *et al.* 1990).

The nonclassical photon statistics of the one-atom maser are observed at a higher flux of atoms or a larger atom–field coupling constant. The $63p_{3/2} \leftrightarrow 61d_{5/2}$ maser transition with $\Omega = 44$ kHz is therefore studied. Experimental results are shown in Fig. 4. Fast atoms with an atom–cavity interaction time of $t_{int} = 35\ \mu$s are used. A very low flux of atoms of $N_{ex} > 1$ is already sufficient to generate a nonclassical maser field. This is the case since the vacuum field initiates a transition of the atom to the lower maser level, thus driving the maser above threshold.

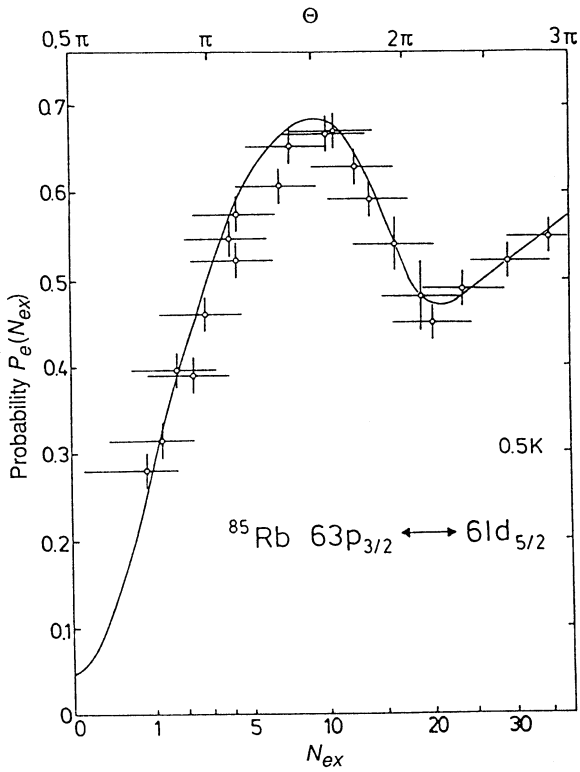

Fig. 5. Probability $P_e(N_{ex})$ of finding the atom in the upper maser level $63p_{3/2}$ for the $63p_{3/2} \leftrightarrow 61d_{5/2}$ transition as a function of the atomic flux.

The sub-Poissonian statistics can be understood from Fig. 5, where the probability of finding the atom in the upper level is plotted as a function of the atomic flux. The oscillation observed is closely related to the Rabi nutation induced by the maser field. The solid curve was calculated according to the one-atom maser theory with a velocity dispersion of 4%. A higher flux generally leads to a higher photon number, but for $N_{ex} < 10$ the probability of finding the atom in the lower level decreases. An increase in the photon number is therefore counterbalanced by the fact that the probability of photon emission in the cavity is reduced. This negative feedback leads to a stabilisation of the photon number (Rempe and Walther 1990). The feedback changes sign at a flux $N_{ex} \approx 10$, where the second maser phase transition is observed at $\Theta = 2\pi$. This is again characterised by large fluctuations of the photon number. Here the probability of finding an atom in the lower level increases with increasing flux. For even higher fluxes, the state of the field is again highly nonclassical. The solid curve in Fig. 4 represents the result of the one-atom maser theory using equation (1) to calculate Q_a. The agreement with experiment is very good. The sub-Poissonian statistics of atoms near $N_{ex} = 30$, $Q_a = 4\%$ and $P_e = 0{\cdot}45$ (see Fig. 5) are generated by a photon field with a variance $\langle N^2\rangle - \langle N\rangle^2 = 0{\cdot}3\langle N\rangle$, which is 70% below the shot noise level. Again, this result agrees with the prediction of the theory (Filipowicz *et al.* 1986*a–c*; Lugiato *et al.* 1987). The mean number of

photons in the cavity is about 2 and 13 in the regions $N_{ex} \approx 3$ and $N_{ex} \approx 30$, respectively. Near $N_{ex} \approx 15$, the photon number changes abruptly between these two values. The next maser phase transition with a super-Poissonian photon number distribution occurs above $N_{ex} \approx 50$.

Sub-Poissonian statistics are closely related to the phenomenon of antibunching, for which the probability of detecting the next event shows a minimum immediately after a triggering event. The duration of the time interval with reduced probability is of the order of the coherence time of the radiation field. In our case this time is determined by the storage time of the photons. The Q_a value therefore depends on the measuring interval T. The measured Q_a value approaches a time-independent value for $T > T_c$. For very short sampling intervals, the statistics of atoms in the lower level show a Poisson distribution. This means that the cavity cannot stabilise the flux of atoms in the lower level on a time scale which is short in relation to the intrinsic cavity damping time.

We emphasise that the reason for sub-Poissonian atomic statistics is the following: a changing flux of atoms changes the Rabi frequency via the stored photon number in the cavity. By adjusting the interaction time, the phase of the Rabi nutation cycle can be chosen so that the probability for the atoms leaving the cavity in the upper maser level increases when the flux and therefore the photon number is raised or vice versa. We observe sub-Poissonian atomic statistics in the case where the number of atoms in the lower state is decreasing with increasing flux and photon number in the cavity. The same argument can be applied to understand the nonclassical photon statistics of the maser field: any deviation of the number of light quanta from its mean value is counterbalanced by a correspondingly changed probability of photon emission for the atoms. This effect leads to a natural stabilisation of the maser intensity by a feedback loop incorporated into the dynamics of the coupled atom–field system.

The experimental results presented here clearly show the sub-Poissonian photon statistics of the one-atom maser field. An increase in the flux of atoms leads to the predicted second maser phase transition. In addition, the maser experiment leads to an atomic beam with atoms in the lower maser level showing number fluctuations which are up to 40% below those of a Poissonian distribution found in usual atomic beams. This is interesting, because atoms in the lower level have emitted a photon to compensate for cavity losses inevitably present under steady-state conditions. But this is a purely dissipative phenomenon giving rise to fluctuations. Nevertheless, the atoms still obey sub-Poissonian statistics.

5. A New Probe of Complementarity in Quantum Mechanics

The preceding section discussed how to generate a nonclassical field inside the maser cavity. But this field is extremely fragile because any attenuation causes a considerable broadening of the photon number distribution. Therefore it is difficult to couple the field out of the cavity while preserving its nonclassical character. But what is the use of such a field? In the present section we want to propose a new series of experiments, performed inside the maser cavity, to test the 'wave–particle' duality of nature, or better said, 'complementarity' in quantum mechanics.

Complementarity (Bohm 1951; Jammer 1974) lies at the heart of quantum mechanics: matter sometimes displays wave-like properties, manifesting themselves

in interference phenomena, and at other times it displays particle-like behaviour, thus providing 'which path' information. No other experiment illustrates this wave–particle duality in a more striking way than the classic Young double-slit experiment (Wootters and Zurek 1979; Wheeler and Zurek 1983). Here we find it impossible to tell which slit light went through while observing an interference pattern. In other words, any attempt to gain 'which path' information disturbs the light so as to wash out the interference fringes. This point has been emphasised by Bohr in his rebuttal to Einstein's ingenious proposal of using recoiling slits (Wheeler and Zurek 1983) to obtain 'which path' information while still observing interference. The physical positions of the recoiling slits, Bohr argued, are only known to within the uncertainty principle. This error contributes a random phase shift to the light beams which destroys the interference pattern.

Such random-phase arguments, illustrating in a vivid way how the 'which path' information destroys the coherent wave-like interference aspects of a given experimental setup, are appealing. Unfortunately, they are incomplete: in principle, and in practice, it is possible to design experiments which provide 'which path' information via detectors which do not disturb the system in any noticeable way. Such 'Welcher Weg' (German for 'which path') detectors have recently been considered within the context of studies involving spin coherence (Englert *et al.* 1988). In the present section we describe a quantum optical experiment (Scully and Walther 1989) which shows that the loss of coherence occasioned by 'Welcher Weg' information, that is, by the presence of a 'Welcher Weg' detector, is due to the establishment of quantum correlations. It is in no way associated with large random-phase factors as in Einstein's recoiling slits.

The details of this application of the micromaser are discussed by Scully *et al.* (1991). Here only the essential features are given. We consider an atomic interferometer where the two particle beams pass through two maser cavities before they reach the two slits of the Young interferometer. The interference pattern observed is then also determined by the state of the maser cavity. The interference term is given by

$$\langle \Phi_1^{(f)}, \Phi_2^{(i)} | \Phi_1^{(i)}, \Phi_2^{(f)} \rangle ,$$

where $|\Phi_j^{(i)}\rangle$ and $|\Phi_j^{(f)}\rangle$ denote the initial and final states of the maser cavity.

Let us prepare, for example, both one-atom masers in coherent states $|\Phi_j^{(i)}\rangle = |\alpha_j\rangle$ of large average photon number $\langle m \rangle = |a_j|^2 > 1$. The Poissonian photon number distribution of such a coherent state is very broad, $\Delta m \approx \alpha \gg 1$. Hence the two fields are not changed much by the addition of a single photon associated with the two corresponding transitions. We may therefore write

$$|\Phi_j^{(f)}\rangle \approx |\alpha_j\rangle ,$$

which to a very good approximation yields

$$\langle \Phi_1^{(f)}, \Phi_2^{(i)} | \Phi_1^{(i)}, \Phi_2^{(f)} \rangle \approx \langle \alpha_1, \alpha_2 | \alpha_1, \alpha_2 \rangle = 1 .$$

Thus there is an interference cross-term different from zero.

When, however, we prepare both maser fields in number states $|n_j\rangle$ (Krause *et al.* 1989; Meystre 1987; Meystre *et al.* 1988) the situation is quite different.

After the transition of an atom to the d-state, that is, after emitting a photon in the cavity the final states read

$$|\Phi_j^{(f)}\rangle = |n_j + 1\rangle$$

and hence

$$\langle \Phi_1^{(f)}, \Phi_2^{(i)} | \Phi_1^{(i)}, \Phi_2^{(f)} \rangle = \langle n_1, n_2 | n_1, n_2 + 1 \rangle = 0\,,$$

that is the coherence cross-term vanishes and no interference is observed.

On first sight this result might seem a bit surprising when we recall that in the case of a coherent state the transition did not destroy the coherent cross-term, i.e. did not affect the interference fringes. However, in the example of number states we can, by simply 'looking' at the one-atom maser state, tell which 'path' the atom took.

It should be pointed out that the beats disappear not only for a number state. For example, a thermal field leads to the same result. In this regard, we note that it is not enough to have an indeterminate photon number to ensure interferences. The state $|\Phi_j^{(f)}\rangle$ goes as $a_j^+|\Phi_j^{(i)}\rangle$ where a_j^+ is the creation operator for the j-th maser. Hence the inner product is

$$\langle \Phi_j^{(i)} | \Phi_j^{(f)} \rangle \rightarrow \langle \Phi_j^{(i)} | a_j^+ | \Phi_j^{(i)} \rangle\,,$$

and in terms of a more general density matrix formalism we have

$$\langle \Phi^{(i)} | \Phi^{(f)} \rangle \rightarrow \sum_n \sqrt{n+1}\, \rho_{n,n+1}^{(i)}\,.$$

Thus we see that an off-diagonal density matrix is needed for the production of interferences. For example, a thermal field having indeterminate photon number would not lead to interference since the photon number distribution is diagonal in this case.

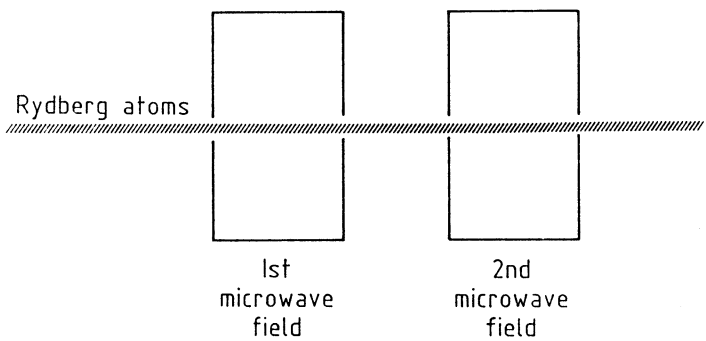

Fig. 6. Setup for the Ramsey experiment.

The atomic interference experiment in connection with one-atom maser cavities is a rather complicated scheme for a 'Welcher Weg' detector. There is a much simpler possibility which we will discuss briefly in the following. This is based

on the logic of the famous 'Ramsey fringe' experiment. In this experiment two microwave fields are applied to the atoms one after the other. The interference occurs since the transition from an upper state to a lower state may either occur in the first or in the second interaction region. In order to calculate the transition probability we must sum the two amplitudes and then square, thus leading to an interference term. We will show here only the principle of this experiment; a more detailed discussion is the subject of another paper (Englert *et al.* 1992). In the setup we discuss here, the two Ramsey fields are two one-atom maser cavities (see Fig. 6). The atoms enter the first cavity in the upper state and are weakly driven into a lower state $|b\rangle$. That is, each microwave cavity induces a small transition amplitude governed by $m\tau$, where m is the atom–field coupling constant and τ is the time of flight across the cavity.

Now if the quantum state of the initial (final) field in the jth cavity is given by $\Phi_j^{(i)}$ ($\Phi_j^{(f)}$), then the state of the atom + maser 1 + maser 2 system at the various relevant times is given in terms of the coupling constant m_j and interaction time τ_j, and the initial $|\Phi_j^{(i)}\rangle$ and final $|\Phi_j^{(f)}\rangle$ states of the jth maser by

$$|\psi(0)\rangle = |a, \Phi_1^{(i)}, \Phi_2^{(i)}\rangle, \qquad |\psi(\tau_1)\rangle \approx |a, \Phi_1^{(i)}, \Phi_2^{(i)}\rangle - im_1\tau_1\,|b, \Phi_1^{(f)}, \Phi_2^{(i)}\rangle\,,$$

$$|\psi(\tau_1+T)\rangle \approx |a, \Phi_1^{(i)}, \Phi_2^{(i)}\rangle - im_1\tau_1\,|b, \Phi_1^{(f)}, \Phi_2^{(i)}\rangle \mathrm{e}^{-i\Delta\omega T}$$

$$|\psi(\tau_1+T+\tau_2) \approx |a, \Phi_1^{(i)}, \Phi_2^{(i)}\rangle - im_1\tau_1\,|b, \Phi_1^{(f)}, \Phi_2^{(i)}\rangle \mathrm{e}^{-i\Delta\omega T} - im_2\tau_2\,|b, \Phi_1^{(i)}, \Phi_2^{(f)}\rangle\,,$$

where $\Delta\omega$ is the atom–cavity detuning, $T \gg \tau_j$ is the time of flight between the two cavities, and a and b denote the lower and upper states of the atoms respectively. If we ask for P_b, the probability that the atom exits cavity 2 in the lower state $|b\rangle$, this is given by

$$\begin{aligned} P_b &= \left[\langle\Phi_1^{(f)}, \Phi_2^{(i)}|m_1^*\tau_1 e^{i\Delta\omega T} + \langle\Phi_1^{(i)}, \Phi_2^{(f)}|m_2^*\tau_2\right] \\ &\quad \times \left[|\Phi_1^{(f)}, \Phi_2^{(i)}\rangle m_1\tau_1 e^{-i\Delta\omega T} + |\Phi_1^{(i)}, \Phi_2^{(f)}\rangle m_2\tau_2\right] \\ &= m_1^*m_1\tau_1^2 + m_2^*m_2\tau_2^2 + (m_1^*m_2\tau_1\tau_2 e^{i\Delta\omega T}\langle\Phi_1^{(f)}, \Phi_2^{(i)}|\Phi_1^{(i)}, \Phi_2^{(f)}\rangle + c.c.)\,. \end{aligned}$$

Now in the usual Ramsey experiment $|\Phi_j^{(i)}\rangle = |\Phi_j^{(f)}\rangle = |\alpha_j\rangle$, where $|\alpha_j\rangle$ is the *coherent state* in the jth maser, which is not changed by the addition of a single photon. Thus the 'fringes' appear going as $\exp(i\Delta\omega T)$. However, consider the situation in which $|\Phi_j^{(i)}\rangle$ is a *number state*, e.g. the state $|0_j^{(i)}\rangle$, having no photons in the jth cavity initially; now we have

$$P = m_1^*m_1\tau_1^2 + m_2^*m_2\tau_2^2 + (m_1^*m_2\tau_1\tau_2\mathrm{e}^{i\Delta\omega T}\langle 1_1, 0_2|\,0_1, 1_2\rangle + c.c.)\,.$$

In this case, the one-atom masers are now acting as 'Welcher Weg' detectors, and the interference term vanishes due to the atom–maser quantum correlation.

We note that the more usual Ramsey fringe experiment involves a strong field '$\pi/2$-pulse' interaction in the two regions. This treatment is more involved than

is necessary for the present purposes. A more detailed analysis of the one-atom maser Ramsey problem is given elsewhere (Englert *et al.* 1992).

We conclude this section by emphasising again that this new and potentially experimental example of wave–particle duality and observation in quantum mechanics displays a feature which makes it distinctly different from the Bohr–Einstein recoiling-slit experiment. In the latter the coherence, that is the interference, is lost due to a phase disturbance of the light beams. In the present case, however, the loss of coherence is due to the correlation established between the system and the one-atom maser. Random-phase arguments never enter the discussion. We emphasise that the argument of the number state not having a well-defined phase is not relevant here; the important dynamics are due to the atomic transition. It is the fact that 'which path' information is made available that washes out the interference cross terms (Scully *et al.* 1991).

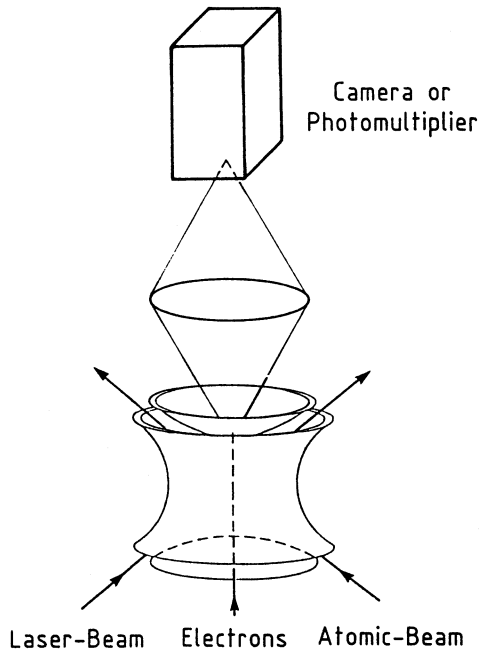

Fig. 7. Sketch of the Paul trap. The fluorescence light is observed through a hole in the upper electrode.

6. The Paul Trap

In contrast to neutral atoms, ions can easily be influenced by electromagnetic fields because of their charge. In most of the experiments the Paul trap is used. It consists of a ring electrode and two end caps as shown in Fig. 7. Trapping can be achieved if time-varying electric fields (Paul *et al.* 1958; Fischer 1959) are applied between the ring and caps (the two caps are electrically connected). A dc voltage in addition changes the relation of the potential depth along the symmetry axis (vertical direction in Fig. 7) to that in a perpendicular direction. The equation of motion of an ion in such a situation is the Mathieu differential equation, well known in classical mechanics which—depending on the voltages applied to the trap (dc and radio-frequency voltages)—allows stable and unstable solutions. Another way to achieve trapping is the use of a constant magnetic

field aligned along the symmetry axis leading to the Penning trap (Wineland *et al.* 1984; Dehmelt 1967). In this case only a dc voltage has to be applied between ring and cap electrodes.

In order to produce the ions in the Paul trap, a neutral atomic beam is directed through the trap centre and ionised by electrons. Unfortunately, the resulting trapped ions have a lot of kinetic energy which renders them useless for most applications, such as spectroscopy; therefore the ions have to be cooled. This is done by laser light. For this purpose the laser frequency ν is tuned below the resonance frequency, so that the energy of the photon is not sufficient to excite the atom. Crudely, the ion can extract the missing energy from its motion and thus reduce its kinetic energy. In other words, the atomic velocity Doppler shifts the atom into resonance to bridge the detuning gap Δ between laser and resonance frequency and the atom absorbs the photon of momentum $\hbar k = h\nu/c$. After the absorption process the momentum of the atom is reduced, lowering its kinetic energy. This leads to a net cooling effect since the re-emission due to atomic fluorescence is isotropic in space. The lowest temperature achievable is determined by the Doppler limit (Dalibard *et al.* 1988) which is in the milliKelvin region. The low temperatures can be obtained within a fraction of a second.

The results discussed in this paper were obtained using a Paul trap with a ring diameter of 5 mm and an end-cap separation of $3 \cdot 54$ mm (Diedrich and Walther 1987; Diedrich *et al.* 1987). This trap is larger than most of the other ion traps used in laser experiments (Wineland *et al.* 1984; Neuhauser *et al.* 1978, 1980). The radio frequency of the field used for dynamic trapping is 11 MHz. The trap is mounted inside a stainless steel, ultrahigh vacuum chamber. We can obtain storage times of hours using a background gas at a pressure of 10^{-10} mbar. The ions are loaded into the trap by means of a thermal beam of neutral atoms (magnesium atoms in our case) which are then ionised close to the centre of the trap by an electron beam entering the trap through a small hole in the lower end-cap (see Fig. 7). In order not to distort the trap potential, the hole is covered by a fine molybdenum mesh. The neutral Mg beam and the laser beam pass through the gaps between the end-cap and the ring electrodes. The laser frequency is shifted by an amount Δ below the $3S_{1/2} \rightarrow 3P_{3/2}$ resonance transition of $^{24}Mg^{+}$ at 280 nm to extract kinetic energy from the ions by radiation pressure as discussed above. In this way, a single ion can be cooled to a temperature below 10 mK. The fluorescence from the ions is observed through a hole in the upper end-cap (see Fig. 7), again covered by a molybdenum mesh. The large size of the trap allows a large solid angle for detecting the fluorescence radiation, either with a photomultiplier or by means of a photon-counting imaging system. To observe the ions, the cathode of the imaging system is placed in the image plane of the microscope objective attached to the trap; in this way images of the ions can be obtained (Blümel *et al.* 1988*a*,*b*).

7. Order versus Chaos: Crystal versus Cloud

The existence of phase transitions in a Paul trap manifests itself by significant jumps in the fluorescence intensity of the ions as a function of the detuning Δ between the laser frequency and the atomic transition frequency. These discontinuities are indicated in Fig. 8 by vertical arrows, and occur between two types of spectra: a broad and a narrow one, analogous to the fluorescence

spectrum of a single, cooled ion. We interpret the broad spectrum as being a fingerprint of an ion cloud and the narrow spectrum as being characteristic of an ordered many-ion situation with a 'single-ion signature'. Thus the jumps clearly indicate a transition from a state of erratic motion within a cloud to a situation where the ions arrange themselves in regular structures. In such a crystalline structure the mutual ion–Coulomb repulsion is compensated by the external, dynamic trap potential. The regime of detunings in which such crystals exist is depicted in Fig. 8 by the horizontal arrow. The existence of the two phases—crystal and cloud—can be verified experimentally by direct observation with the help of a highly sensitive imaging system, and theoretically by analysing ion trajectories via Monte Carlo computer simulations (Blümel *et al.* 1988*a*,*b*).

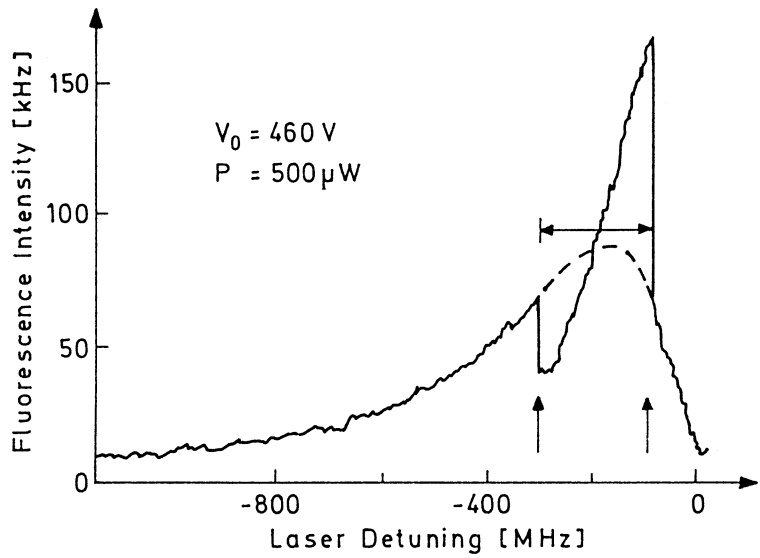

Fig. 8. Fluorescence intensity, that is, photon counts per second, from five ions as a function of the laser detuning Δ. The vertical arrows indicate the detunings where phase transitions occur. The horizontal arrow shows the range of detunings in which a stable five-ion crystal is observed. The spectrum was scanned from left to right.

The excitation spectrum of Fig. 8 and the jumps in it were recorded by altering the detuning Δ from large negative values to zero. When we scan the spectrum in the opposite direction the jumps occur at different values of Δ, which means there is hysteresis associated with these phase transitions (Blümel *et al.* 1988*a*). Such hysteresis behaviour can be expected with laser-cooled ions because the cooling power of the laser strongly depends upon the details of the velocity distribution of the ions. The behaviour of the ions in the trap is governed by the trap voltage, the laser detuning, and the laser power. Hysteresis loops appear whenever one of these parameters is changed up or down whilst the others are kept constant.

Fig. 9 shows the ion structures as measured with the imaging system. For these measurements only a radio-frequency voltage was applied to the trap electrodes: in this case the potential is a factor of two deeper along the symmetry axis than perpendicular to it, and therefore plane ion structures are observed being perpendicular to the symmetry axis (for details see Blümel *et al.* 1988*a*,*b*).

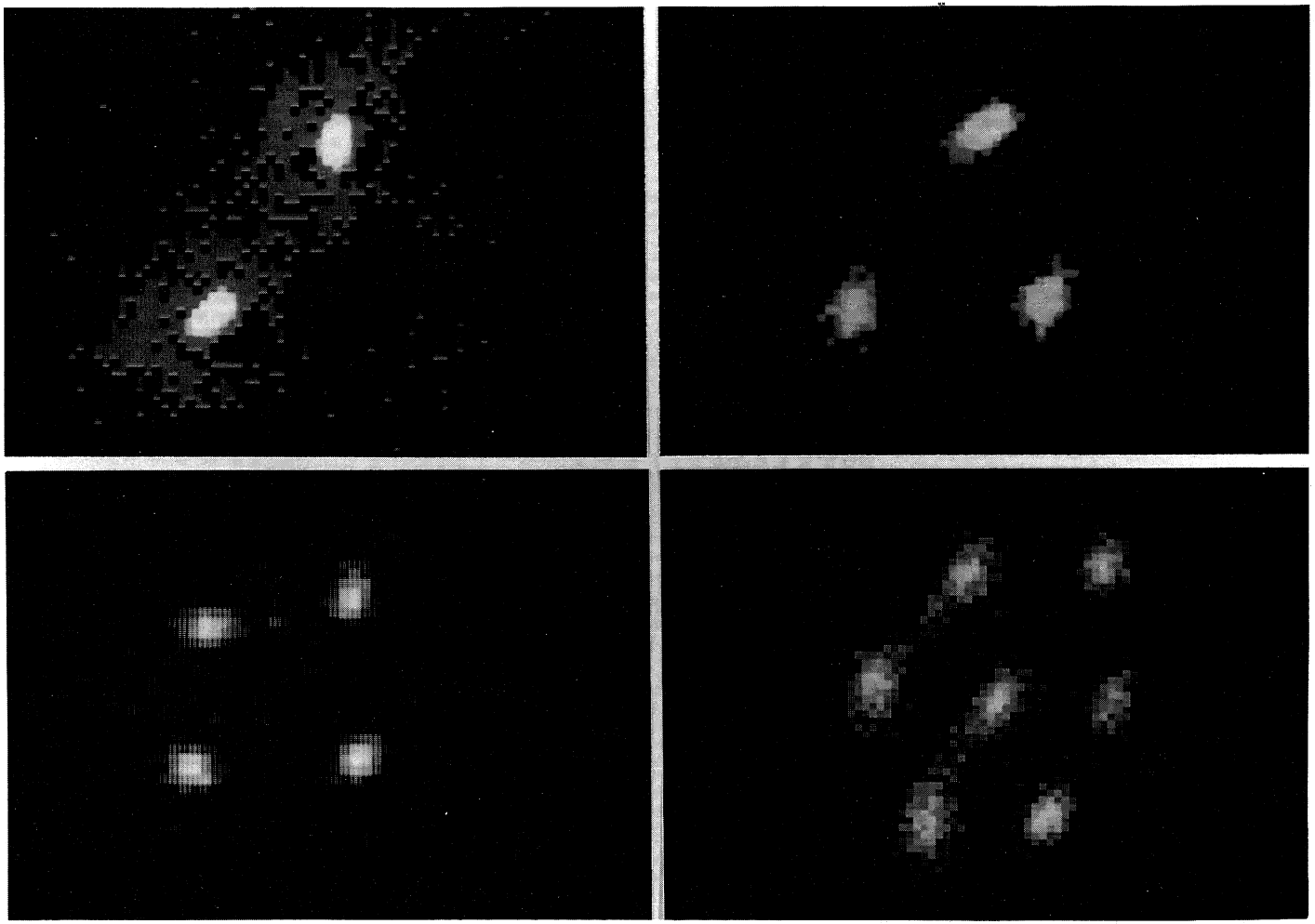

Fig. 9. Two, three, four and seven ions confined by the dynamical potential of a Paul trap and crystallised into an ordered structure in a plane perpendicular to the symmetry axis of the trap. The average separation of the ions is 20 μm.

Once we have accepted the existence of ion crystals and the corresponding phase transitions, we must ask how do they actually occur? Would the cooling laser not force any cloud immediately to crystallise? A heating mechanism balancing the cooling effect of the laser must be the answer to this puzzle, but what heating mechanism? Since the early days of Paul traps this so-called radio-frequency heating has repeatedly been cited (Wineland *et al.* 1984). A deeper understanding however was missing and was provided only recently by a detailed study of the dependence of the cloud → crystal and crystal → cloud phase transitions on the relevant parameters (Blümel *et al.* 1988*a*,*b*, 1989).

The ions are subjected to essentially four different forces: the first one arising from the trapping field, then the Coulomb interaction between the ions, the laser cooling force, and finally a random force arising from the spontaneously emitted photons. Using these forces computer simulations of the motion of the ions can be performed (Blümel *et al.* 1988*a*). Depending on the external parameters such as the laser power, the laser detuning, and the radio-frequency voltage, the

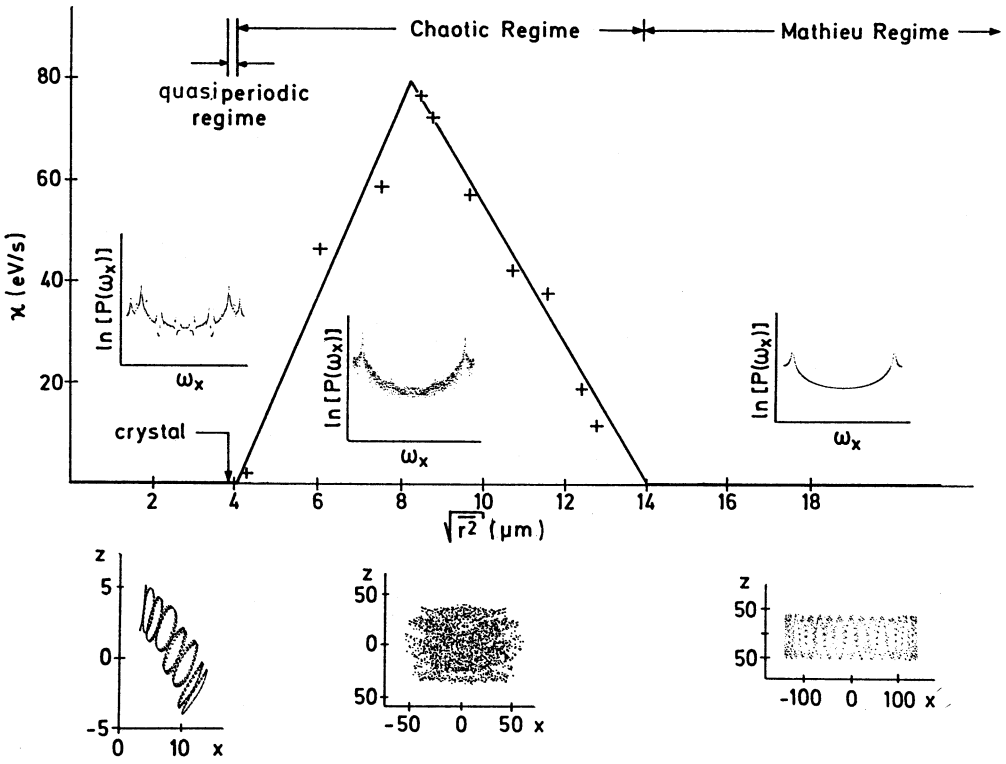

Fig. 10. Average heating rate κ of five ions in a Paul trap versus mean ion separation. The insets show the power spectrum and the corresponding stroboscopic Poincaré sections (plane perpendicular to the symmetry axis) of the mean relative separation of the ions in three characteristic domains: the crystal state, the chaotic regime, and the Mathieu regime. The units on the axes are in μm. In order to calculate the power spectrum of the 'crystal' shown on the left-hand side, the distance between the five ions was changed by 1 μm from the equilibrium position. The Mathieu regime shown on the right is dominated by the secular motion.

experimentally observed phenomena could be reproduced (Blümel *et al.* 1988*a*). Some of the results of the simulations are summarised in Fig. 10. Plotted is the radio-frequency heating parameter κ of five ions versus their mean separation (Blümel *et al.* 1989). For zero laser power and large r, we did not observe any net heating of the ions. This is confirmed by our experiments in which, even in the absence of a cooling laser, large clouds of ions can be stored in a Paul trap over several hours without being heated out of the trap. When the ions are far apart, the Coulomb force is small, and on short time scales the ions behave essentially like independent single stored ions. For this reason, we call this part of the heating diagram the 'Mathieu regime' (Blümel *et al.* 1988*a*, 1989). Turning on a small laser, the rms radius r reduces drastically, but comes to a halt at about 14 μm. At this distance the nonlinear Coulomb force between the ions plays an important role and the motion of the ions gets chaotic. In this situation the power spectrum of the ions becomes a continuum leading to a radio-frequency heating process.

Increasing the laser power further results in an even smaller cloud. The smaller cloud produces more chaotic radio-frequency heating, as can be seen clearly from the negative slope of the heating curve in the range $8 < r < 14$ μm. Finally, in the range $4 < r < 8$ μm there is still chaotic heating but the slope of the heating curve is positive. As a consequence of the resulting triangular shape of the heating curve at a laser power of about $P = 150$ μW, corresponding to $r \approx 8$ μm, the chaotic heating power can no longer balance the cooling power of the laser light and the cloud collapses into the crystalline state located at $r \approx 3{\cdot}8$ μm. At this point the amplitude of the ion motion is so small that the nonlinear part of the repulsive Coulomb force is negligible again, so that chaotic heating disappears and the phase transition occurs.

Due to this collapse of the cloud state, the behaviour of the heating rate in the range $3{\cdot}8 < r < 8$ μm cannot be studied by balancing laser cooling and radio-frequency heating. In this case we start out from the crystal state and slightly displace the ions to explore the vicinity of the crystal. We observe no heating for $3{\cdot}8 < r < 4$ μm, but quasiperiodic motion, and thus dub this regime the 'quasiperiodic' regime. We call the upper edge of the quasiperiodic regime ($r \approx 4$ μm) the 'chaos threshold'. An initial condition beyond the chaos threshold, i.e. satisfying $r \approx 4$ μm, leads to heating and expansion of the ion configuration; numerical data relevant for the shape of the heating curve can be taken during this expansive phase. The laser power P is set to zero for this type of experiment. We conjecture that—apart from the trivial case of a single stored ion—the heating curve is universal, i.e. its qualitative shape, including the existence of the chaotic regime, does not depend on the number of simultaneously trapped ions, and even applies to systems as remotely connected as, for example, Rydberg atoms in strong electromagnetic fields.

For the quasiperiodic, the chaotic, and the Mathieu regimes, respectively, we display the corresponding type of power spectrum as the insets above the abscissa in Fig. 10. The data were actually taken for the case of two ions, but would not look much different in the five-ion case. We obtain a discrete spectrum in the quasiperiodic regime and a complicated noisy spectrum in the chaotic regime. The spectrum in the Mathieu regime is again quite simple and is dominated by the secular motion frequency. We also show stroboscopic pictures of the

locations of the ions in the plane perpendicular to the symmetry axis of the trap characterising the three regions (insets below the abscissa in Fig. 10).

As a function of increasing rf voltage, the chaos threshold moves towards the radius of the crystalline configuration. However, before the chaos threshold reaches the crystal radius, the equations of motion of the ions become unstable in the direction of the symmetry axis, indicating that in this particular situation the particles would fall out of the trap. In order to achieve proper melting without losing particles, the crystal radius has to be enlarged artificially by noise so that the size of the distorted crystal overlaps the region of chaotic heating. Proper melting without the assistance of noise should be possible if we start in a quasiperiodic state typified in the bottom left inset of Fig. 10. Such configurations have a larger radius in the beginning, and the chaos threshold could be reached before the onset of the single-particle Mathieu instability, which would not be the case otherwise (Blümel *et al.* 1989).

8. The Ion Storage Ring

A completely new era of accelerator physics could begin if it were possible to produce, store and accelerate Coulomb crystals in particle accelerators and storage rings. To work with crystals instead of the usual dilute, weakly coupled particle clouds has at least one advantage: the luminosity of accelerators (storage rings) could be greatly enhanced, and (nuclear) reactions whose cross sections are too small to be investigated in currently existing accelerators would become amenable to experimentation.

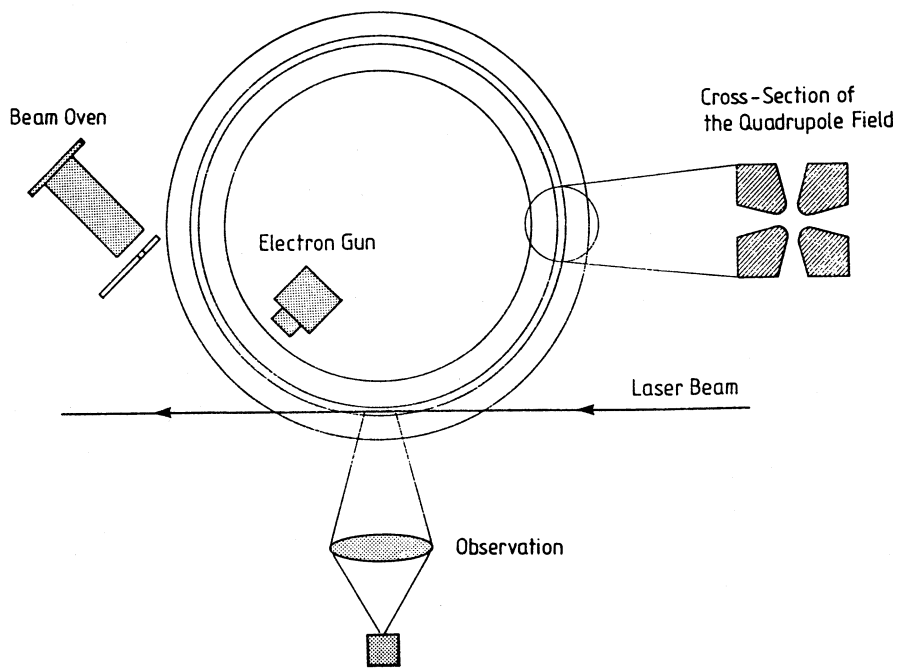

Fig. 11. Quadrupole storage ring. The cross section of the electrode configuration is shown in the insert on the right. The diameter of the ring is 113 mm and the distance between the electrodes is 5 mm.

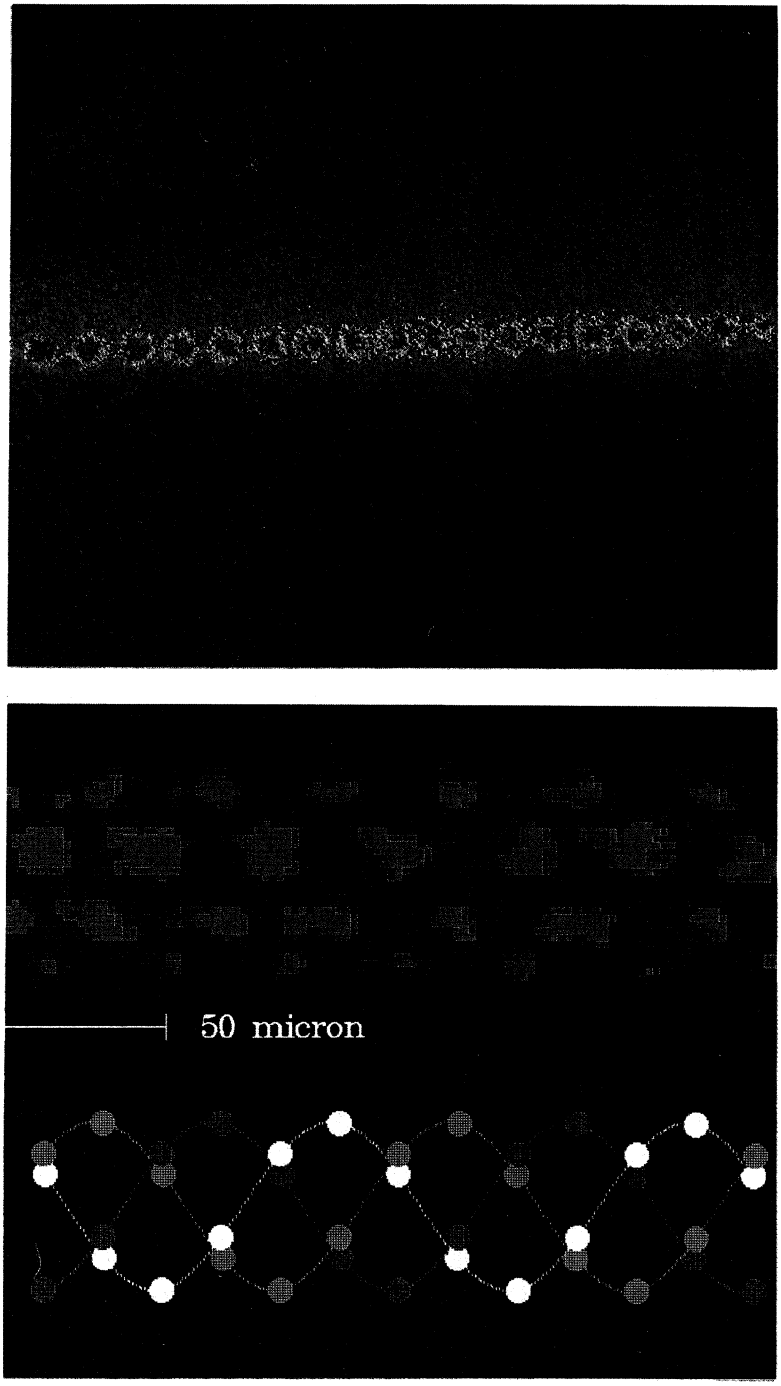

Fig. 12. Ordered structures of Mg^+ ions in a quadrupole trap. *Upper part*: linear structure with a distance between the ions of about 25 μm. The image is colour-coded, with red indicating high and blue indicating low intensity. *Lower part*: Helical structure consisting of three interwoven helices shown in different colours below. The closely appearing pairs of ions sit on opposite sites, resulting in twice the intensity at those positions (Waki *et al.* 1992).

In the following, we would like to discuss very briefly our recent experiments using a miniature quadrupole storage ring. The storage ring is similar to the one described by Drees and Paul (1964) or by Church (1969). We can observe phase transitions of the stored ions, and the observed ordered ion structures are quite similar to the ones expected in relativistic storage rings; they are, however, much easier to achieve. The motivation for building this small storage ring came from the fact that micromotion perturbs the ion structures in a Paul trap and only a single trapped ion is free of micromotion (Wineland *et al.* 1984). The ring trap used consists of a quadrupole field, leading to harmonic binding of the ions in a plane transverse to the electrodes of the quadrupole and no confinement along the axis (see Fig. 11). Confinement along the axis is achieved, however, by the Coulomb interaction between the ions when the ring is filled; then the total number of ions in the ring determines the average distance between them.

A schematic of the ring trap used for our experiments is shown in Fig. 11 (Walther 1991; Waki *et al.* 1992). It consists of four electrode rings shown in the insert on the right. The hyperbolic cross section of the electrodes required for an ideal quadrupole field was approximated by a circular one. These experiments were also performed with Mg^+ ions. The ions were produced between the ring electrodes by ionising the atoms of a weak atomic beam, produced in an oven which injected the atoms tangentially into the trap region. The electrons used for the ionisation came from an electron gun, the electron beam of which was perpendicular to the direction of the atomic beam. A shutter in front of the atomic beam oven allowed the interruption of the atomic flux. The ultrahigh vacuum chamber was pumped by an ion getter pump. After baking the chamber a vacuum of 10^{-10} mbar could be reached. Under these conditions the number of ions stored in the trap stayed practically constant for several hours.

When laser cooling of the ions is started a sudden change in the fluorescence intensity is observed, resembling very much that seen with stored ions in a Paul trap (Fig. 8) which indicates a phase transition and the formation of an ordered structure of ions. The ion structure can also be observed using an ultrasensitive imaging system. Pictures of typical ion structures are shown in Fig. 12. The ions are excited by a frequency-tunable laser beam which enters the storage ring tangentially. In the linear configuration the ions are all sitting in the centre of the quadrupole field; therefore they do not show micromotion and it is possible to cool them further to temperatures in the microKelvin region. The new cooling methods proposed by Dalibard *et al.* (1988) can be applied to the Mg^+ ions so that the single-photon recoil limit can be achieved for the cooling process. At this limit the kinetic energy of the ions is smaller than the energy resulting from the 'zero-energy' motion of the harmonically bound ions; the ion structure then reaches its vibrational ground state, i.e. a Mössbauer situation is generated. This means that the recoil limit does not exist anymore. The ion structure then corresponds to a Wigner crystal. We conclude by noting that the observed ion configurations in the quadrupole ring trap are described in a recent paper by Birkl *et al.* (1992).

References

Birkl, G., Kassner, S., and Walther, H. (1992). *Nature* **357**, 310.

Blümel, R., Chen, J. M., Quint, W., Schleich, W., Shen, Y. R., and Walther, H. (1988*a*). *Nature* **334**, 309.

Blümel, R., Chen, J. M., Diedrich, F., Peik, E., Quint, W., Schleich, W., Shen, Y. R., and Walther, H. (1988*b*). 'Atomic Physics' **11** (Eds S. Haroche *et al.*), p. 243 (World Scientific Publishing: Singapore).

Blümel, R., Kappler, C., Quint, W., and Walther, H. (1989). *Phys. Rev.* A **40**, 808.

Bohm, D. (1951). 'Quantum Theory' (Prentice Hall: Englewood Cliffs).

Carmichael, H. J., and Walls, D. F. (1976). *J. Phys.* B **9** L43, 1199.

Chu, S., Bjorkholm, J. E., Ashkin, A., and Cable, A. (1986). 'Atomic Physics' **10** (Eds H. Narumi and S. Shimamura), p. 377 (North-Holland: Amsterdam).

Church, D. A. (1969). *J. Appl. Phys.* **40**, 3127.

Cresser, J. D., Häger, J., Leuchs, G., Rateike, M., and Walther, H. (1982). 'Dissipative Systems in Quantum Optics' **21** (Springer: Berlin).

Dalibard, J., Salomon, C., Aspect, A., Arimondo, E., Kaiser, R., Vansteenkiste, N., and Cohen-Tannoudji, C. (1988). 'Atomic Physics' **11** (Eds S. Haroche *et al.*), p. 199 (World Scientific Publishing: Singapore).

Dehmelt, H. G. (1967). 'Advances in Atomic and Molecular Physics' **3** (Eds D. R. Bates and I. Estermann), pp. 53–72 (Academic: New York).

Diedrich, F., Peik, E., Chen, J. M., Quint, W., and Walther, H. (1987). *Phys. Rev. Lett.* **59**, 2931.

Diedrich, F., and Walther, H. (1987). *Phys. Rev. Lett.* **58**, 203.

Drees, J., and Paul, W. (1964). *Z. Phys.* **180**, 340.

Eberly, J. H., Narozhny, N. B., and Sanchez-Mondragon, J. J. (1980). *Phys. Rev. Lett.* **44**, 1323.

Englert, B.-G., Schwinger, J., and Scully, M. O. (1988). *Found. Phys.* **18**, 1045.

Englert, B.-G., Walther, H., and Scully, M. O. (1992). *Appl Phys.* B **54**, 366.

Filipowicz, P., Javanainen, J., and Meystre, P. (1986*a*). *Opt. Comm.* **58**, 327.

Filipowicz, P., Javanainen, J., and Meystre, P. (1986*b*). *Phys. Rev.* A **34**, 3077.

Filipowicz, P., Javanainen, J., and Meystre, P. (1986*c*). *J. Opt. Soc. Am.* B **3**, 906.

Fischer, E. (1959). *Z. Phys.* **156**, 1.

Gallas, J. A., Leuchs, G., Walther, H., and Figger, H. (1985). 'Advances in Atomic and Molecular Physics' **20** (Eds D. Bates and B. Bederson), p. 413 (Academic: New York).

Haroche, S., and Raimond, J. M. (1985). 'Advances in Atomic and Molecular Physics' **20** (Eds D. Bates and B. Bederson), p. 350 (Academic: New York).

Jammer, M. (1974). 'The Philosophy of Quantum Mechanics' (Wiley: New York).

Jaynes, E. T., and Cummings, F. W. (1963). *Proc. IEEE* **51**, 89.

Kimble, H. J., Dagenais, M., and Mandel, L. (1977). *Phys. Rev. Lett.* **39**, 691.

Krause, J., Scully, M. O., and Walther, H. (1987). *Phys. Rev.* A **36**, 4547.

Krause, J., Scully, M. O., Walther, T., and Walther, H. (1989). *Phys. Rev.* A **39**, 1915.

Loudon, R., and Knight, P. L. (1987). *J. Mod. Opt.* **34**, 707.

Lugiato, L., Scully, M. O., and Walther, H. (1987). *Phys. Rev.* A **36**, 740.

Mandel, L. (1979). *Opt. Lett.* **4**, 205.

Meschede, D., Walther, H., and Müller, G. (1985). *Phys. Rev. Lett.* **54**, 551.

Meystre, P. (1987). *Opt. Lett.* **12**, 669.

Meystre, P., Rempe, G., and Walther, H. (1988). *Opt. Lett.* **13**, 1078.

Neuhauser, W., Hohenstatt, M., Toschek, P., and Dehmelt, H. (1978). *Phys. Rev. Lett.* **41**, 233.

Neuhauser, W., Hohenstatt, M., Toschek, P., and Dehmelt, H. (1980). *Phys. Rev.* A **22**, 1137.

Paul, W., Osberghaus, O., and Fischer, E. (1958). 'Ein Ionenkäfig' **415** (Forschungsberichte des Wirtschafts- und Verkehrsministeriums Nordrhein-Westfalen).

Pritchard, D. E., Helmerson, K., and Martin, A. G. (1988). 'Atomic Physics' **11** (Eds S. Haroche *et al.*), p. 179 (World Scientific Publishing: Singapore).

Rempe, G., Schmidt-Kaler, F., and Walther, H. (1990). *Phys. Rev. Lett.* **64**, 2783.

Rempe, G., and Walther, H. (1990). *Phys. Rev.* A **42**, 1650.

Rempe, G., Walther, H., and Klein, N. (1987). *Phys. Rev. Lett.* **58**, 353.

Scully, M. O., Englert, B.-G., and Walther, H. (1991). *Nature* **351**, 111.

Scully, M. O., and Walther, H. (1989). *Phys. Rev.* A **39**, 5229.

Short, R., and Mandel, L. (1983). *Phys. Rev. Lett.* **51**, 384.

Slosser, J. J., Meystre, P., and Wright, E. M. (1990). *Opt. Lett.* **15**, 233.

Slusher, R. E., Hollberg, L. W., Yurke, B., Mertz, J. C., and Valley, J. F. (1985). *Phys. Rev. Lett.* **55**, 2409.
Waki, I., Kassner, S., Birkl, G., and Walther, H. (1992). *Phys. Rev. Lett.* **68**, 2007.
Walls, D. F. (1979). *Nature* **280**, 451.
Walls, D. F. (1983). *Nature* **306**, 141.
Walls, D. F. (1986). *Nature* **324**, 210.
Walther, H. (1991). 'Proc. Workshop on Light Induced Kinetic Effects on Atoms, Ions and Molecules' (Eds L. Moi *et al.*) (ETS Editrice: Pisa).
Wheeler, J. A., and Zurek, W. H. (1983). 'Quantum Theory and Measurement' (Princeton University Press).
Wineland, D. J., Itano, W. M., Bergquist, J. C., Bollinger, J. J., and Prestage, J. D. (1984). 'Atomic Physics' **9** (Eds R. S. van Dyck Jr and E. N. Fortson) (World Scientific Publishing: Singapore).
Wootters, W., and Zurek, W. (1979). *Phys. Rev.* D **19**, 473.

Manuscript received 31 March, accepted 25 June 1992